DESIGN AND EXPERIMENT OF A BUILT-IN SCREEN-TYPE CYCLONE SEPARATION CLEANING SYSTEM FOR A SMALL-SCALE WHEAT COMBINE HARVESTER

/

小型小麦联合收获机内置筛网式旋风分离清选系统设计与试验

Yangang LI [1)], Xiaoyu CHAI [1)], Jinpeng HU [1)], Zhiqiang SONG [1)], Yuzhe WANG [1)], Lizhang XU [1,*)]

[1)] College of Agricultural Engineering, Jiangsu University, Zhenjiang 212013, China

**Corresponding author's Email: justxlz@ujs.edu.cn*

DOI: https://doi.org/10.35633/inmateh-76-92

Keywords: *Small Combine Harvester; Wheat; Cleaning System; Screen; CFD-DEM*

ABSTRACT

To address the issues of high grain impurity rate and low cleaning efficiency in the cyclone separation cleaning system of small wheat combines harvesters in hilly and mountainous areas, this study proposes an internally screened cyclone separation cleaning system. Using the CFD-DEM coupled simulation method, the effect of the screen structure on the motion trajectory and separation behavior of the threshed material was systematically analyzed. A response surface methodology was applied to analyze the impact of interaction factors on cleaning performance. The optimal working parameters were determined to be: fan speed of 4020 r/min, scraper shaft speed of 340 r/min, clearance between the screen and the chamber wall of 37 mm, and mesh size of 29 mm. Under these parameters, the simulation results showed a grain impurity rate of 2.99% and a cleaning loss rate of 1.10%, while the field experiment results were 3.08% and 1.14%, respectively. The field experiment results indicate that the designed cleaning system improved the cleaning performance and operational efficiency of the small combine harvester, providing both theoretical support and engineering guidance for the optimized design of cleaning system in small combine harvesters for hilly regions.

摘要

针对丘陵山区小型联合收获机旋风分离清选系统小麦清选时籽粒含杂率高、清选效率低等问题，本文提出一种内置筛网式旋风分离清选系统。采用 CFD-DEM 耦合仿真方法，系统分析筛网结构对脱出物运动轨迹及分离规律的影响。并采用响应面试验方法，分析了各交互因素对清选性能的影响，得出优化工作参数组合为：风机转速 4020 r/min、刮板转轴转速 340 r/min、筛网到筒壁间隙 37 mm、网格间距 29 mm。在此参数组合下，仿真结果显示籽粒含杂率为 2.99%，清选损失率为 1.10%；田间试验为籽粒含杂率 3.08%，清选损失率 1.14%。田间试验结果表明，所设计清选系统提高了小型联合收获机的清选性能与作业效率，为丘陵山区小型联合收获机清选系统的优化设计提供了理论依据与工程指导。

INTRODUCTION

Hilly and mountainous areas are important regions for the production of grains and specialty agricultural products in China, with the arable land in these areas accounting for 34.62% of the total arable land in the country. However, due to the terrain constraints, the promotion and application of large combine harvesters in these areas face significant challenges *(Mandler et al., 2025)*. Small combine harvesters (with a feeding rate of less than 1.5 kg/s) have become one of the main pieces of equipment in hilly and mountainous areas, thanks to their compact structure and flexible operation. Among these, the cleaning system, as a key component of the harvester, directly affects the overall performance of the machine *(Ding et al., 2022)*. Small combine harvesters generally use cyclone separation cleaning systems *(Wan et al., 2018)*, which rely solely on airflow to separate grains from impurities. When the proportion of impurities in the discharged material, such as wheat, is high, these systems often face issues such as high impurity rates and low cleaning efficiency, limiting the overall machine performance and requiring targeted optimization.

Yangang Li, Student; Xiaoyu Chai, Lecturer; Jinpeng Hu, Student; Zhiqiang Song, Lecturer; Yuzhe Wang, Student; Lizhang Xu, Professor.

For air-sieve cleaning system *Mirzazadeh et al, (2022)* used response surface methodology to optimize the mathematical model of feed rate, fan speed, and sieve opening. *Lovchikov and Ognev (2022)* analyzed the impact of screen type and airflow velocity on cleaning efficiency, providing theoretical support for the optimization of cleaning systems. *Badretdinov et al. (2022)* used mathematical modeling to analyze the impact of uneven airflow distribution on cleaning performance and proposed an improvement plan. For the cyclone separation cleaning device of small combine harvesters, *Liu et al. (2015)* designed an airflow-based cleaning device for wheat harvesting, but field tests could only meet the feeding rate requirement below 0.5 kg/s. *Bizuneh and Abate (2024)* studied the performance of cyclone separators for peas and lentils, analyzing their efficiency in impurity separation and cleaning. *Shi et al. (2022)* proposed a compound cleaning system and optimized the internal flow field for flax harvesting in hilly terrain. *Shu et al. (2024)* improved cyclone cleaning systems with airflow feeding for rapeseed harvesting. These studies indicate that air-sieve cleaning systems are well-developed and have good cleaning performance, but the large size and complex structure of such systems make them difficult to apply in small combine harvesters with limited space. Small combine harvesters generally use blower or pneumatic conveying combined with cyclone separation, which can only meet the feeding rate requirements below 0.5 kg/s when processing high-impurity crops. Although compound cleaning systems have improved efficiency, their complex structure still limits their widespread application in small machines.

In summary, this study proposes an internally screened cyclone separation cleaning system. The system ensures stable and orderly material feeding through the scraper conveyor and optimizes the separation path of impurities by combining the synergistic effect of the screen and airflow. Using CFD-DEM coupled simulations, the impact of the screen structure on the motion trajectory and separation behavior of the threshed material was analyzed. The optimal parameter combination for the cleaning system was determined through response surface methodology, and its performance was verified through field experiments. This study provides theoretical support and engineering guidance for the optimized design of cleaning systems for small combine harvesters in hilly and mountainous areas.

MATERIALS AND METHODS

Overall Structure and Working Principle

The overall structure of combine harvester

This study focuses on the 4LZ-1.0LC combine harvester, which is equipped with a KD1100FB4-2 National IV diesel engine. The harvester primarily consists of a double-layer cutting and feeding system, a conveying system, a threshing system, a cleaning system, a power drive system, a crawler walking system, and a hydraulic control system. The main structure is shown in Fig. 1, and the key technical specifications are listed in Table 1.

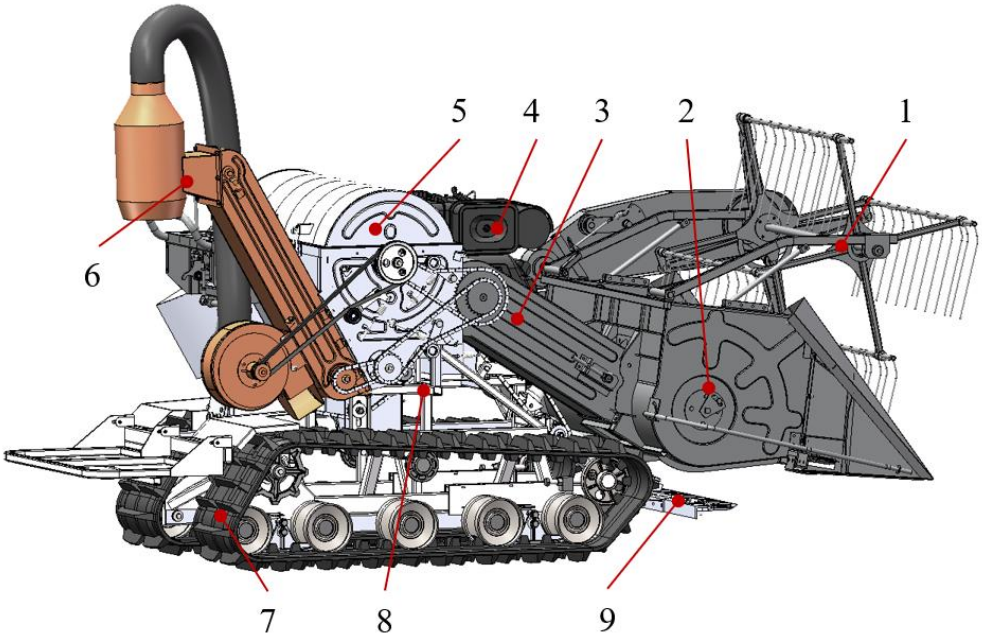

Fig. 1 - Schematic diagram of the structure of small wheat combine harvester

1 - Reel; 2 – Header; 3 - Spiral conveyor; 4 – Engine; 5 - Threshing system; 6 - Cleaning system; 7 - Crawler track; 8 - Chassis frame; 9 - Lower cutter

Table 1

Main parameters of combine harvester

Item	Parameter
Structure Type	Full-feed, crawler-type
Engine Power/kW	9.8
Dimensions (L×W×H)/mm	3100×1500×1700
Total Weight/kg	645
Cutting Platform Clearance/mm	1200
Rated Feeding Amount/(kg/s)	1.0
Operating Speed/(m/s)	0.4~1.2
Production Efficiency/(hm^2/h)	≥0.06

Structure and working principle of the cleaning system

To address the poor cleaning performance of conventional airflow-based cleaning systems when processing discharged material with a high proportion of impurities, this study proposes an internally screened cyclone separation cleaning system. As shown in Fig. 2, the system mainly consists of a scraper conveyor, a separation chamber, a screen, and a centrifugal impurity-extraction fan. During operation, the threshed wheat mixture is uniformly fed into the separation chamber at a constant speed under the action of the scraper conveyor. Light impurities are directly carried out of the chamber by the high-speed airflow. Stalks and other heavier impurities are constrained by the screen and lifted upward by the continuous airflow before being discharged. In contrast, the grains pass through the screen and fall along the chamber wall to the grain outlet, thereby achieving effective separation of grains and impurities.

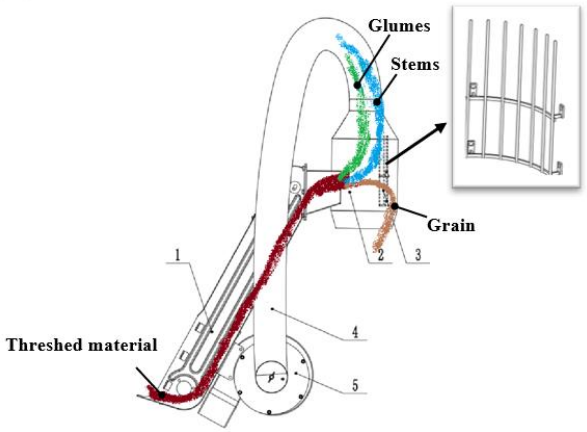

Fig. 2 - Cleaning system structure and working principle diagram

1 - Scraper conveying; 2 - Separation cylinder; 3 – Screen; 4 - Suction pipe; 5 - Suction centrifugal fan

Dynamic and kinematic analysis of threshed material

As shown in Fig. 3, the airflow in the separation chamber flows upward, with higher airflow velocities in the upper and lower conical sections and lower velocities near the chamber walls.

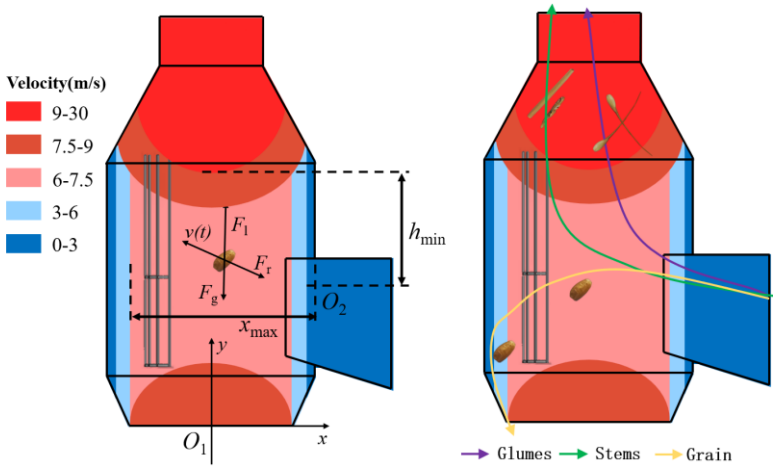

Fig. 3 - Schematic diagram of the force and motion analysis of the threshed material

When the threshed material is conveyed into the separation chamber at a certain speed by the scraper, the forces acting on it can be expressed as follows:

$$\begin{cases} F_r = -kv(t) \\ F_l = kv_{air}(x(t), y(t)) \\ F_g = -mg \end{cases} \quad (1)$$

In the equation, F_r represents the aerodynamic drag force, N; F_l represents the lift force generated by the airflow, N; F_g represents the gravitational force, N; k represents the aerodynamic drag coefficient; m is the mass of the threshed material, kg; g is the gravitational acceleration, 9.81 m/s².

The motion velocity of the threshed material can be expressed as:

$$\begin{cases} m\dfrac{dv_x}{dt} = -k\left(v_x(t) - u(x(t), y(t))\right) \\ m\dfrac{dv_y}{dt} = -k\left(v_y(t) - v(x(t), y(t))\right) - mg \end{cases} \quad (2)$$

The displacement expression can be obtained by integrating the velocity:

$$\begin{cases} x(t) = x_0 + \int_0^t v_x(\tau)d\tau \\ y(t) = y_0 + \int_0^t v_y(\tau)d\tau \end{cases} \quad (3)$$

To achieve effective separation of impurities from the threshed material, the impurities must reach the high-speed airflow region in the upper conical section before entering the low-speed airflow region on the left side. Therefore, their motion trajectory must satisfy the following conditions:

$$\begin{cases} |x(t_f) - x_0| < x_{max} \\ y(t_f) - y_0 \geq h_{min} \end{cases} \quad (4)$$

In the equation, x_{max} represents the maximum horizontal displacement of the impurities, m; h_{min} represents the minimum vertical displacement of the impurities, m.

By combining the above velocity and motion equations, the integral expression for the motion of the threshed material is obtained as follows:

$$\begin{cases} \left| \int_0^{t_f} \left[v_{x0} + \int_0^{\tau} \left(-\dfrac{k}{m}(v_x(s) - u(x(s), y(s))) \right) ds \right] d\tau \right| < x_{max} \\ \int_0^{t_f} \left[v_{y0} + \int_0^{\tau} \left(-\dfrac{k}{m}(v_y(s) - v(x(s), y(s))) - g \right) ds \right] d\tau \geq h_{min} \end{cases} \quad (5)$$

After adding a properly sized screen to the separation chamber, the screen blocks the horizontal movement of impurities. At this point, the forces and displacement of the impurities are expressed as follows:

$$\begin{cases} \vec{F}_l = k_l(t)\vec{v}_{air}(x(t), y(t)) \\ \vec{F}_g = -mg\vec{j} \end{cases} \qquad \begin{cases} x(t) = 0 \\ y(t) = y_{t_0} + \int_{t_0}^{t} v_y(\tau)d\tau \end{cases} \quad (6)$$

In the equation, t_0 represents the time taken for the impurities to reach the screen, *s*.

The above analysis indicates that the motion trajectory of the threshed material in the airflow field is jointly influenced by its physical properties, the airflow distribution, and its initial velocity and position. By installing a screen in the separation chamber, the horizontal displacement of impurities is restricted while being expelled upward under the action of high-speed airflow, thereby improving separation efficiency.

Design of Key Components

Separation chamber

As shown in Fig. 4, the performance of the separation chamber is primarily determined by the airflow rate and the diameter of the separation chamber. The required airflow rate for cleaning, Q, is given by the equation 7 *(Geng et al., 2011; Zhao et al., 2024)*:

$$Q = \frac{\gamma q}{\mu \rho} \quad (7)$$

In the equation, γ represents the proportion of impurities in the total feeding rate of the harvester; q represents the feeding rate, kg/s; ρ represents the air density, kg/m³; μ represents the concentration ratio of the airflow carrying impurities.

The diameter of the middle section of the separation chamber and the diameter of the grain outlet are determined by the following equations:

$$D = \sqrt{\frac{4Q}{\pi V}} \tag{8}$$

In the equation, V represents the airflow velocity inside the separation chamber, m/s.

Based on calculations and the overall machine layout, the diameter of the middle section of the separation chamber was determined to be D = 225 mm, the diameter of the grain outlet was 190 mm, and the total height of the separation chamber was 440 mm.

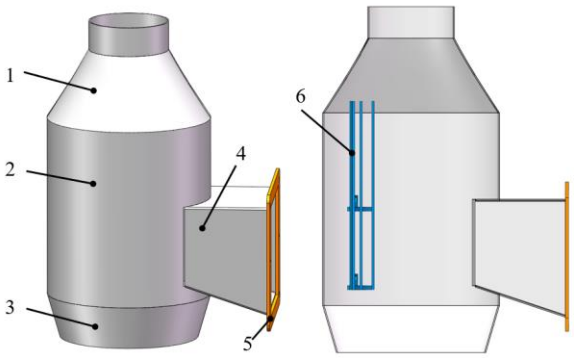

Fig. 4 - Schematic diagram of the separation cylinder structure

1 - Upper conical section; 2 - Middle section; 3 - Lower conical section; 4 - Feeding section; 5 - Connecting flange; 6 - Screen

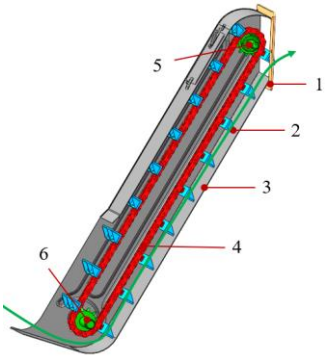

Fig. 5 - Structure diagram of scraper conveyor

1 - Discharge flange; 2 – Scraper; 3 – Housing; 4 – Chain; 5 - Driven shaft and sprocket; 6 - Driving shaft and sprocket

Scraper conveyor

Based on the overall spatial layout of the harvester and practical application requirements, a bottom-scraping type scraper conveyor was selected. Its structure is shown in Fig. 5.

To prevent blockage in the scraper conveyor and ensure smooth material conveying, the discharge outlet length *l* is determined by the following equation *(Geng et al., 2011)*:

$$l = v_g \sqrt{\frac{2H_t \cos\varphi}{g\cos(\beta+\varphi)}} \tag{9}$$

In the equation, v_g represents the conveying speed of the scraper, 1.5 m/s; H_t represents the lifting height of the threshed material, m. β represents the inclination angle of the conveyor relative to the horizontal plane; φ represents the friction angle between the material and the scraper.

The conveying capacity of the scraper conveyor is determined by the following equation:

$$Q_w = L_g B_g v_g m_g \psi k_1 \tag{10}$$

In the equation, L_g, B_g represents the length and width of the scraper, m; m_g represents the bulk density of the material, kg/m³; ψ represents the filling coefficient; k_1 represents the inclination coefficient.

After calculation and considering the actual structure of the combine harvester, the scraper length is 125 mm, width is 25 mm, the discharge outlet length *l* is 150 mm, and the inclination angle is 30°.

Coupled Simulation of CFD-DEM

CFD and DEM model establishment

To ensure that the simulation reflects real-world conditions while reducing computational load, the simulation model retained the fan and scraper conveyor components but shortened the conveying stroke of the scraper. After constructing the flow channel model of the cleaning system in SolidWorks, the model was exported in .x_t format and imported into the Workbench Mesh module. An unstructured tetrahedral mesh, suitable for complex geometries, was used for meshing the flow channel. Local mesh refinement was applied to the geometrically complex regions, such as the screen and fan blades.

A total of 762, 707 mesh elements were generated. The mesh quality was evaluated to be satisfactory, meeting the simulation requirements. The mesh is shown in Fig. 6.

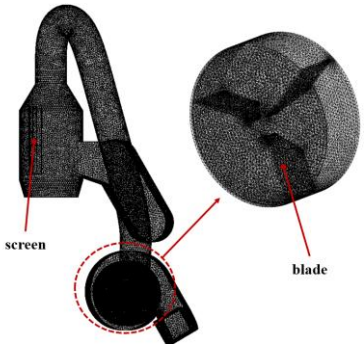

Fig. 6 - Meshing

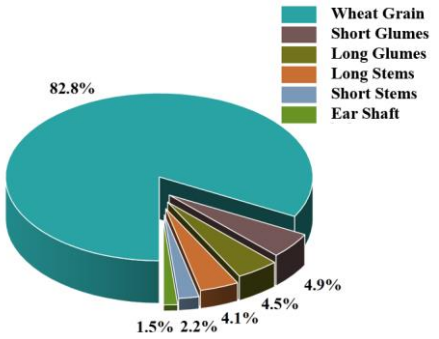

Fig. 7 - Mass ratio of threshed material

Based on field experiment measurements, the mass proportions of different components in the threshed wheat material from the small combine harvester were obtained, as shown in Fig. 7. Given the significant proportion of glumes, this study incorporated a glume model into the existing discrete element modeling of wheat grains and stems by previous scholars to enhance the reliability of the simulation. *(Schramm and Tekeste, 2022; Wiącek et al., 2023)*. The average geometric dimensions of the components were measured using a vernier caliper, and DEM models for each component were constructed in EDEM, as shown in Fig. 8. The material property parameters for the particle models, including material density, Poisson's ratio, and shear modulus, were set based on the research team's existing data *(Li, 2017)*. A particle factory was established on the scraper, with the following particle generation rates: grains at 436.71 g/s, long stems at 21.62 g/s, short stems at 11.60 g/s, rachis at 7.91 g/s, long glumes at 23.73 g/s, and short glumes at 25.84 g/s.

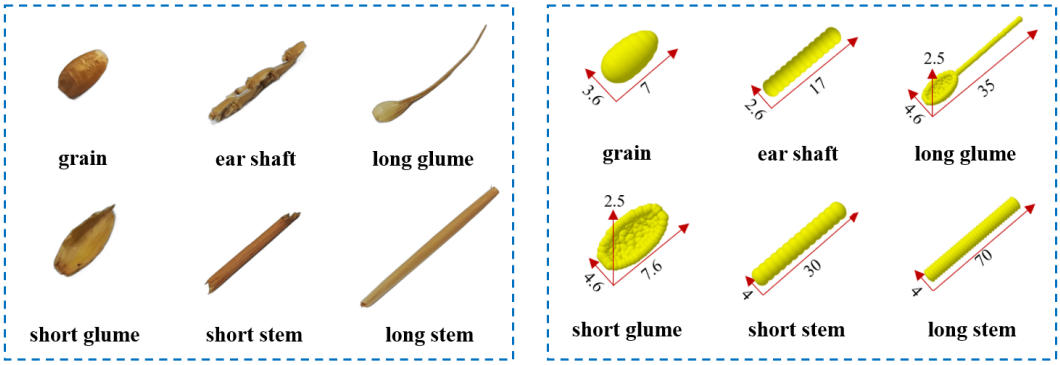

Fig. 8 - DEM model of threshed material

Parameter setting of CFD-DEM

In Fluent, the standard turbulence model was employed, and the mesh region corresponding to the centrifugal impurity-extraction fan impeller was defined as a Multiple Reference Frame rotational zone *(Zhou et al., 2025; Mircea et al., 2020)*, with a set rotational speed of 4000 r/min. The inlet boundary of the airflow in the cleaning system was set as a pressure inlet, while the outlet was set as a pressure outlet. In EDEM, the motion parameters of the scraper were defined according to a scraper shaft speed of 350 r/min. The contact interactions between particles and between particles and geometry were modeled using the Hertz-Mindlin (no slip) contact model and the Standard Rolling Friction model. The Eulerian model was used for the numerical simulation of gas-solid two-phase flow. After multiple tests, the EDEM time step was set to 5×10^{-7} s and the Fluent time step was set to 5×10^{-5} s. A total of 30,000-time steps were calculated, with a total simulation time of 1.5 s.

Simulation Test of Response Surface Method

Based on Section 2.1.3 and the simulation analysis results, fan speed, scraper shaft speed, the clearance between the screen and the separation chamber wall, and the screen mesh size were selected as experimental factors, with grain impurity rate Y_1 and cleaning loss rate Y_2 as the evaluation indices. The coding of each experimental factor is shown in Table 2.

A four-factor, three-level response surface experiment was designed using the Box-Behnken method *(Ayorinde and Owolarafe, 2023; Kushwah et al., 2023)*.

Table 2

Test factor level and coding table

Code	Factor			
	Fan Speed X_1/(r/min)	Scraper Shaft Speed X_2/(r/min)	Screen Gap X_3/(mm)	Grid Spacing X_4/(mm)
-1	3600	300	30	15
0	4000	400	45	25
1	4400	500	60	35

RESULTS AND ANALYSIS

Simulation Results and Analysis

Airflow field analysis

After the simulation was completed, the vertical central plane and several horizontal cross-sections at different heights of the separation chamber were extracted in CFD-Post to obtain airflow velocity contour maps, as shown in Fig. 9.

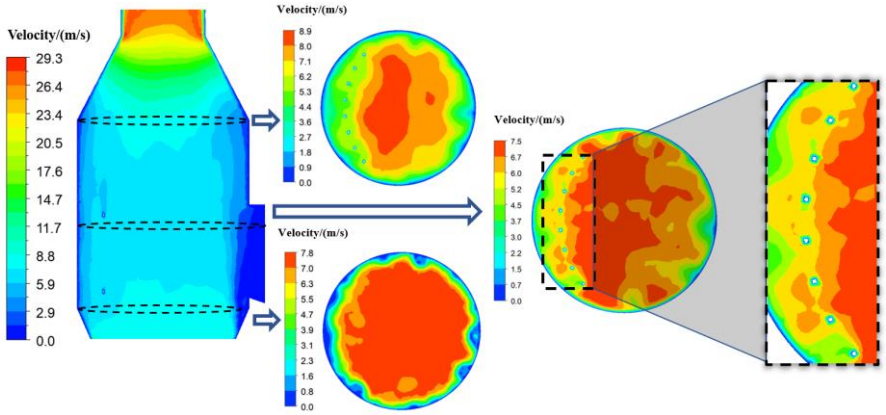

Fig. 9 - Velocity cloud diagram of different sections of the separation cylinder

Overall, the airflow field exhibited distinct high- and low-velocity regions: the airflow velocity was relatively high in the upper and lower conical sections, relatively uniform in the middle section, and significantly lower near the chamber walls. The spatial distribution characteristics of the airflow field were generally consistent with the initial design expectations, verifying the rationality of the separation chamber structure. The airflow velocity on the right side of the screen was significantly higher than on the left. The high-velocity region on the right side facilitates efficient separation of grains and impurities, while the low-velocity region on the left promotes rapid sedimentation of the grains.

Screen function analysis

To clarify the specific functional mechanism of the screen during the cleaning process, a comparative analysis was conducted between the material motion near the left wall of the separation chamber under the no-screen condition and the motion on both sides of the screen when the screen was installed. The particle motion in the selected regions is shown in Fig. 10.

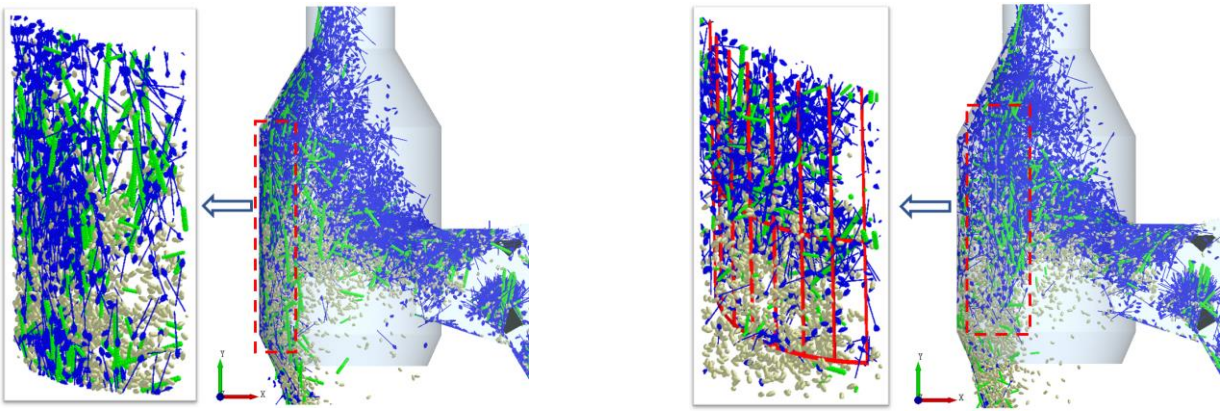

(a) Without Screen *(b) With Screen*

Fig. 10 - Analysis of particle movement in cleaning process

Fig. 10(a) shows the particle motion under the no-screen condition. After the threshed material is conveyed into the separation chamber by the scraper, a large amount of glumes, along with some rachis and stalks, is directly extracted by the airflow, while a considerable amount of material accumulates along the chamber wall. In the selected chamber wall region, both impurities and grains are discharged together through the grain outlet, resulting in poor cleaning performance. Fig. 10(b) illustrates the particle motion with the screen installed. In the extracted screen region, only a small amount of impurities passes through the screen. Most impurities are blocked by the screen and remain within the central high-speed airflow region, which reduces mixing with grains and allows more impurities to be extracted by the airflow.

To further quantify the impact of the screen structure on cleaning performance, two particle mass statistics regions were defined in the EDEM post-processing: one below the grain outlet and the other above the impurity outlet. These were used to calculate the grain impurity rate and cleaning loss rate. The simulation results showed that, without the screen, the impurity rate was 5.23% and the cleaning loss rate was 1.09%; after installing the screen, the impurity rate decreased to 3.10%, while the loss rate remained stable at 1.07%. In summary, the screen structure effectively optimized the movement path of large-particle impurities such as stalks, improving the separation efficiency between grains and impurities, and reducing the impurity rate by more than 40%.

Analysis of the centroid velocity of threshed material particles

To further analyze the motion behavior of the threshed material during the cleaning process, and in consideration of the working characteristics of the separation chamber, this study focuses on the variation pattern of centroid velocity in the Y direction (vertical direction). Since analyzing individual particles involves a high degree of subjectivity and cannot fully represent the motion characteristics of an entire particle type, the Y-direction velocity vectors of all threshed material particles within the separation chamber were extracted over time. The summed velocity vectors were used to generate time-series curves of the centroid velocity in the Y direction for each particle group.

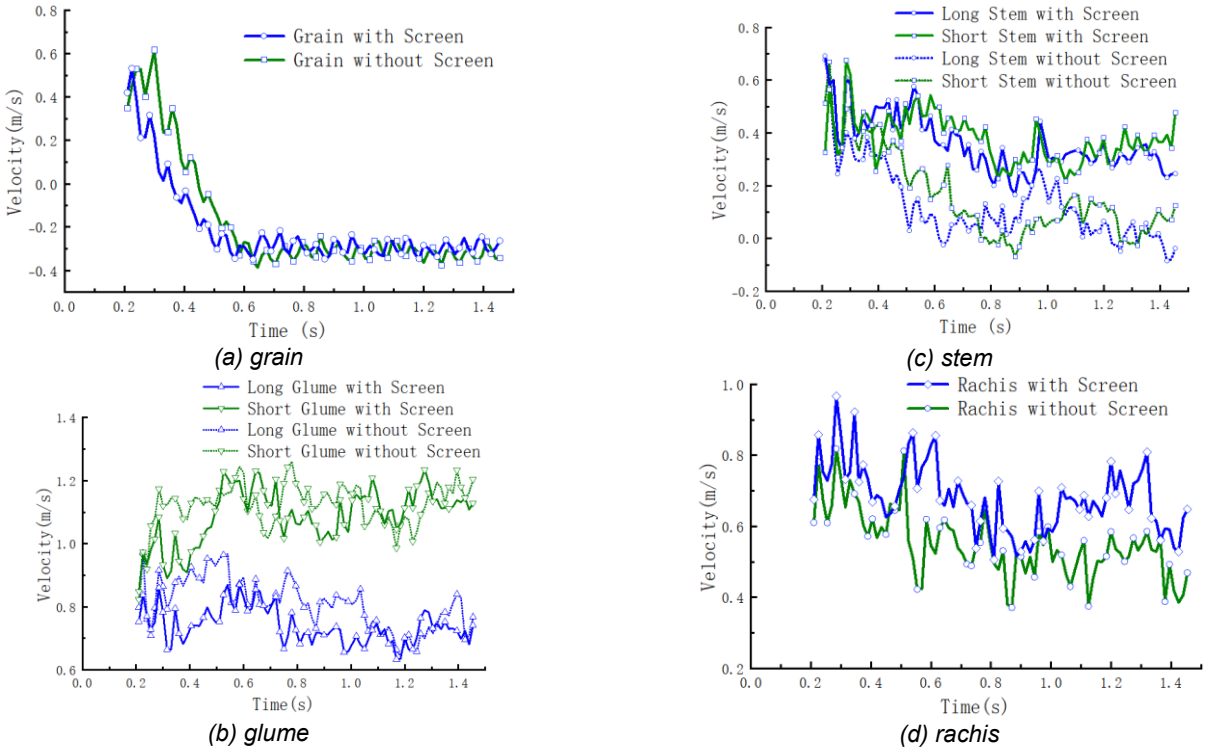

Fig. 11 - Relationship between the velocity of particle swarm centroid motion and time in the Y direction

As shown in Fig. 11(a), it takes 0.2 s for the wheat grains to move from the particle factory to the separation chamber, and after 0.6 s, the velocity gradually stabilizes. Once the cleaning process stabilizes, the grain velocity under both conditions becomes nearly identical, indicating that the screen structure has a minimal effect on grain movement, and the grains can easily pass through the screen. As shown in Fig. 11(b), under both conditions, the velocity of short glumes gradually increases after entering the separation chamber and stabilizes, indicating that after entering the chamber, short glumes are quickly expelled upward through the impurity outlet under the action of airflow. The velocity of long glumes decreases after cleaning stabilizes.

Combining this with the analysis of the cleaning simulation process, under the no-screen condition, a large amount of impurities accumulate in the left region of the separation chamber, leading to the difficulty in expelling some glumes, which results in a reduced overall glume velocity. As shown in Fig. 11(c) and Fig. 11(d), in the screen-equipped cleaning system, the centroid velocity of the rachis and stem particles in the Y direction is higher than that under the no-screen condition. The average velocities of stems and rachis during the stable phase were calculated: under the no-screen condition, the velocities of the rachis, long stems, and short stems were 0.51 m/s, 0.06 m/s, and 0.07 m/s, respectively; under the screen-equipped condition, the corresponding velocities were 0.65 m/s, 0.2 m/s, and 0.24 m/s, representing increases of 27.45%, 233.33%, and 242.86%, respectively.

In summary, the screen structure significantly increased the upward velocity of the rachis and stems, effectively improving the separation efficiency between grains and impurities and enhancing the overall cleaning performance of the cleaning device.

Analysis of Response Surface Experiment Results

Regression model building and testing

The results of the response surface experiment are shown in Table 3. Based on the response surface experimental data, variance analysis was performed on the regression models for the impurity rate Y_1 and cleaning loss rate Y_2. The analysis results are shown in Table 4. The quadratic polynomial regression models for Y_1 and Y_2 are:

$$Y_1 = 2.97 - 1.85X_1 + 0.22X_2 + 0.73X_3 - 0.17X_4 - 0.11X_1X_2 - 0.3X_1X_3 + 0.09X_1X_4 + 0.2X_1^2 + 0.76X_2^2 + 0.87X_3^2 + 0.92X_4^2 \quad (11)$$

$$Y_2 = 1.45 + 0.85X_1 + 0.40X_2 + 0.23X_3 - 0.25X_4 + 0.24X_1X_2 + 0.13X_1X_3 - 0.1X_1X_4 + 0.21X_1^2 + 0.06X_2^2 + 0.1X_3^2 \quad (12)$$

Table 3

Results of response surface experiment

Experiment	X_1	X_2	X_3	X_4	Y_1/%	Y_2/%	Experiment	X_1	X_2	X_3	X_4	Y_1/%	Y_2/%
1	-1	0	-1	0	4.96	0.75	15	0	1	0	1	4.68	1.55
2	0	0	-1	1	3.88	1.08	16	0	0	0	0	3.03	1.42
3	-1	1	0	0	6.04	1.01	17	0	-1	1	0	5.05	1.38
4	0	1	0	-1	5.11	2.12	18	1	0	0	-1	2.21	2.82
5	1	0	0	1	2.11	1.96	19	1	0	-1	0	1.84	2.25
6	0	-1	0	1	4.25	0.93	20	-1	0	1	0	6.86	1.03
7	0	-1	0	-1	4.61	1.25	21	0	0	-1	-1	4.12	1.5
8	0	0	0	0	2.91	1.48	22	-1	0	0	1	5.71	0.68
9	0	-1	-1	0	3.59	1.03	23	0	0	0	0	2.96	1.45
10	0	1	1	0	5.61	2.33	24	-1	-1	0	0	5.45	0.65
11	0	0	1	1	5.32	1.42	25	1	0	1	0	2.56	3.04
12	1	1	0	0	2.21	3.25	26	0	1	-1	0	3.99	1.74
13	-1	0	0	-1	6.17	0.94	27	1	-1	0	0	2.04	1.94
14	0	0	1	-1	5.75	1.94							

Table 4

Analysis of variance for regression equations

Source	Impurity Rate of Grain					Cleaning Loss Rate				
	Sum of Squares	DF	Mean Square	F	P	Sum of Squares	DF	Mean Square	F	P
Model	56.58	14	4.04	601.41	<0.0001**	12.75	14	0.91	229.87	<0.0001**
X_1	41.14	1	41.14	6122.5	<0.0001**	8.67	1	8.67	2188.40	<0.0001**
X_2	0.59	1	0.59	87.08	<0.0001**	1.94	1	1.94	488.67	<0.0001**
X_3	6.41	1	6.41	953.76	<0.0001**	0.65	1	0.65	163.73	<0.0001**
X_4	0.34	1	0.34	50.60	<0.0001**	0.73	1	0.73	183.05	<0.0001**
X_1X_2	0.044	1	0.04	6.56	0.0249*	0.23	1	0.23	56.95	<0.0001**
X_1X_3	0.35	1	0.35	51.80	<0.0001**	0.065	1	0.065	16.41	0.0016**
X_1X_4	0.032	1	0.032	4.82	0.0485*	0.090	1	0.090	22.72	0.0005**
X_2X_3	0.0064	1	0.0064	0.95	0.3484	0.014	1	0.014	3.63	0.0808
X_2X_4	0.0012	1	0.0012	0.18	0.6770	0.016	1	0.016	3.94	0.0704
X_3X_4	0.0090	1	0.0090	1.34	0.2691	0.0025	1	0.0025	0.63	0.4424
X_1^2	0.21	1	0.21	31.22	0.0001**	0.23	1	0.23	57.73	<0.0001**
X_2^2	3.06	1	3.06	454.89	<0.0001**	0.02	1	0.02	5.61	0.0354*
X_3^2	4.03	1	4.03	600.13	<0.0001**	0.057	1	0.057	14.37	0.0026**

Source	Impurity Rate of Grain					Cleaning Loss Rate				
	Sum of Squares	DF	Mean Square	F	P	Sum of Squares	DF	Mean Square	F	P
X_4^2	4.50	1	4.50	669.30	<0.0001**	0.0187	1	0.0187	4.71	0.0507
Residual	0.081	12	0.0067			0.048	12	0.0040		
Lack of fit	0.073	10	0.0073	2.02	0.3763	0.046	10	0.0046	5.08	0.1755
Pure Error	0.0073	2	0.0036			0.0018	2	0.0009		
Cor Total	56.66	26				12.80	26			

Note: ** indicates extremely significant difference (P ≤ 0.01); * indicates significant difference (P ≤ 0.05).

As shown in Table 4, the p-value of the regression models for grain impurity rate and cleaning loss rate is less than 0.0001, indicating that the model is highly significant overall. The p-value for the lack-of-fit term is greater than 0.05, suggesting that the fitted quadratic regression equation matches well with the actual data. For the grain impurity rate, the effects of X_1, X_2, X_3, X_4, X_1X_3, X_1^2, X_2^2, X_3^2 and X_4^2 were extremely significant. For the cleaning loss rate, the effects of X_1, X_2, X_3, X_4, X_1X_2, X_1X_3, X_1X_4, X_1^2 and X_3^2 were extremely significant. According to the magnitude of the regression coefficients, the order of importance of the factors affecting the grain impurity rate was: fan speed, clearance between the screen and the separation chamber wall, scraper shaft speed, and screen mesh size. For the cleaning loss rate, the order of influence was: fan speed, scraper shaft speed, screen mesh size, and clearance between the screen and the chamber wall.

Influence of interaction factors on cleaning performance

To visually analyze the impact of interaction factors on the grain impurity rate and cleaning efficiency, response surface plots of the regression model were generated, as shown in Fig. 12 and Fig. 13.

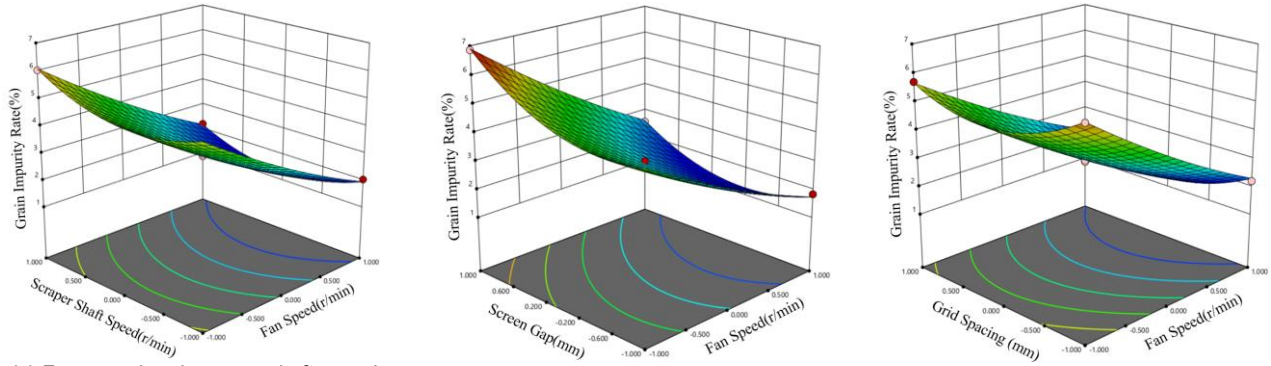

(a) Fan speed and scraper shaft speed *(b) Fan speed and screen gap* *(c) Fan speed and grid spacing*

Fig. 12 - The influence of interactive factors on the impurity content rate of grains

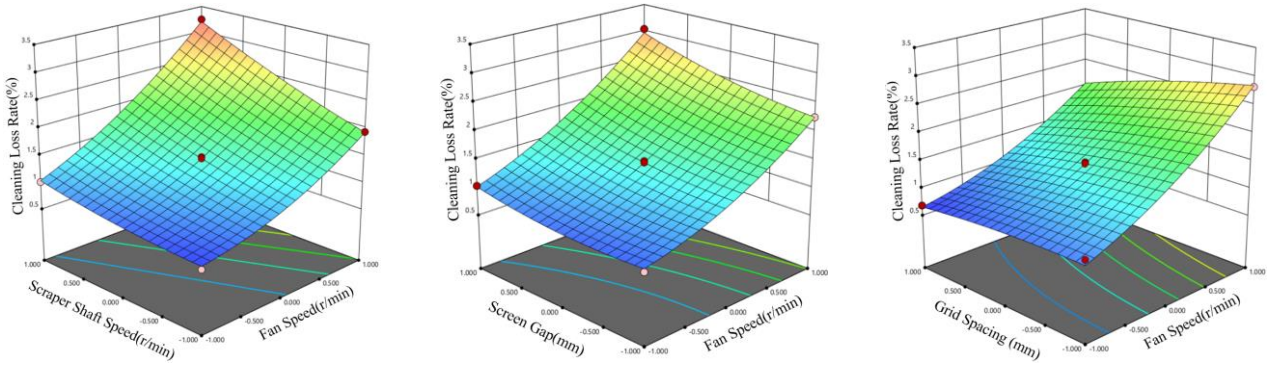

(a) Fan speed and scraper shaft speed *(b) Fan speed and screen gap* *(c) Fan speed and grid spacing*

Fig. 13 - The influence of interactive factors on the cleaning loss rate

The optimal working parameters are determined

To further improve cleaning performance, the minimum values of grain impurity rate and cleaning loss rate were used as optimization indices. Considering that small combine harvesters focus more on reducing the loss rate, weights of 0.4 and 0.6 were assigned to the grain impurity rate and cleaning loss rate, respectively. Under the constraint conditions of the experimental factor levels, target optimization was performed to determine the optimal working parameters. The regression model was optimized to solve for the target parameters. Considering practical factors, the optimal working parameter combination was determined as follows: fan speed of 4020 r/min, scraper shaft speed of 340 r/min, clearance between the

screen and the chamber wall of 37 mm, and mesh size of 29 mm. Three repeated simulation tests were conducted under this parameter combination, yielding an average grain impurity rate of 2.99% and an average cleaning loss rate of 1.10%.

Field Experiment Verification

To verify the cleaning performance of the cleaning device under the optimal working parameters in hilly and mountainous areas, a field experiment was conducted from May 8 to 11, 2024, in Shehong City, Sichuan Province, according to the relevant provisions of GB/T 8097-2008 Test Methods for Combine Harvesters and JB/T 13544-2018 Micro Full-Feed Combine Harvesters. The wheat variety used in the experiment was “Chuannong 30,” with an average plant height of 823 mm, a thousand-kernel weight of 45.1 g, and a grain moisture content of 18.12%. The experimental field was divided into three straight 15-meter sections. The combine harvester operated at full cutting width and a constant speed. Grains were collected below the grain outlet using woven bags, and impurities were collected using nylon mesh bags. After each test, the collected materials were separated, and the weight of each component was measured using a high-precision electronic scale. The grain impurity rate and cleaning loss rate were then calculated. The test procedure is shown in Fig. 14. The experiment results are shown in Table 5.

Fig. 14 - Field experiment and cleaning performance

Table 5

Field experiment results

Experiment Number	Collected Material Mass (g)	Collected Grain Mass (g)	Loss Mass (g)	Impurity Rate (%)	Loss Rate (%)
1	8538.53	8290.68	94.71	2.90	1.13
2	9433.63	9142.91	97.58	3.08	1.06
3	9237.78	8936.88	110.55	3.26	1.22

The average grain impurity rate was 3.08%, and the cleaning loss rate was 1.14%. Compared to the simulation results, the relative error for the impurity rate was 2.92%, and the relative error for the loss rate was 3.51%. These errors mainly arise from the complexity of field environmental factors and differences in operator performance. Overall, the relative errors were small, indicating that the simulation model has high accuracy and reliability. This validates the effectiveness and feasibility of the designed built-in screen cyclone separation cleaning system in improving cleaning performance and operational efficiency.

CONCLUSIONS

To address the issues of high grain impurity rates and low cleaning efficiency in small combine harvesters during wheat harvesting, an internally screened cyclone separation cleaning system is proposed. This system combines the synergistic effects of the screen and airflow, effectively improving the separation efficiency between grains and impurities, as well as the overall cleaning performance. Through CFD-DEM coupled simulation technology, the impact of the screen structure on the motion trajectory and separation behavior of the threshed material was systematically analyzed. Using response surface methodology, regression models were established for the factors and evaluation indices, and the optimal working parameter combination was determined: fan speed of 4020 r/min, scraper shaft speed of 340 r/min, clearance between the screen and the chamber wall of 37 mm, and mesh size of 29 mm. Under this parameter combination, the simulation results showed a grain impurity rate of 2.99% and a cleaning loss rate of 1.10%. Field test results showed a grain impurity rate of 3.08% and a cleaning loss rate of 1.14%, verifying the accuracy of the simulation model. The designed cleaning device meets the wheat cleaning performance standards for small combine harvesters in hilly and mountainous areas.

ACKNOWLEDGEMENT

Key R&D Program of Shandong Province, China(2022SFGC0201); The National Natural Science Foundation of China (52405271), and The Natural Science Foundation of Jiangsu Province (BK20230544).

REFERENCES

[1] Ayorinde, T. A., Owolarafe, O. K. (2023). Effect of operational parameters on the performance of a kenaf harvester. *Spanish Journal of Agricultural Research, Vol. 21*(4), pp. e0209-e0209. https://orcid.org/0000-0002-6748-8704

[2] Badretdinov, I. D., Mudarisov, S. G. & Khaliullin, D. T. (2022). Examination of the Airflow Uneven Distribution over the Combine Harvester Cleaning System. *Mathematical Modelling of Engineering Problems*, *Vol. 9*(2), pp. 371-378. https://doi.org/10.18280/mmep.090210

[3] Bizuneh, Y. E. Abate, L. A. (2024). Experimental investigation on the separation and cleaning efficiency of pea & lentil split chaffs using cyclone cleaner. *Case Studies in Thermal Engineering*, *Vol. 61*, pp. 104875. https://doi.org/10.1016/j.csite.2024.104875

[4] Ding, B., Liang, Z., Qi, Y., Ye, Z. & Zhou, J. (2022). Improving cleaning performance of rice combine harvesters by DEM–CFD coupling technology. *Agriculture*, *Vol. 12*(9), pp. 1457. https://doi.org/10.3390/agriculture12091457

[5] Geng, D., Zhang, D., Wang, X. & Yang, Z. (2011). *New Edition of Agricultural Machinery Science* (新编农业机械学). Beijing: National Defense Industry Press. *(In Chinese)*. ISBN: 9787118075281.

[6] Kushwah, A., Sharma, P. K., Mani, I., Kushwaha, H. L., Sahoo, R. N., Sarkar, S. K., Sharma, B. B., Carpenter, G., Singh, N., Yadav. R., Nag, R. H. (2023). Parameter optimization for selective harvesting in cauliflower (Brassica oleracea) using response surface methodology. *The Indian Journal of Agricultural Sciences*, *Vol. 93*(8), pp. 912-918. https://doi.org/10.56093/IJAS.V93I8.136898

[7] Li Y. (2017). Numerical simulation and experiment of gas-solid two-phase flow in multi-duct cleaning device (多风道清洗装置中气固两相流的数值模拟与试验). *Zhenjiang: Jiangsu University*. *(In Chinese).*

[8] Liu, Z., Zheng, Y., Wang, Z., Chen, D., Wang, J. (2015). Study on airflow cleaning device of micro rice-wheat combine harvester (微型稻麦联合收获机气流式清选装置研究). *Transactions of the Chinese Society for Agricultural Machinery*, *Vol. 46*(7), pp. 102-108. *(In Chinese).* https://doi.org/10.6041/j.issn.1000-1298.2015.07.016

[9] Lovchikov, A.P., Ognev, I.I. (2022). Theoretical background for combination of sieves of combine harvester cleaning system. *AIP Conference Proceedings*. *AIP Publishing, Vol. 2503*(1). https://doi.org/10.1063/5.0099726

[10] Mandler, A., Becce, L., Carabin, G., Gronauer, A., Mazzetto, F. (2025). Mechanisation of Mountain Farming. Observations on Grain Production in the Alps. In: Sartori, L., Tarolli, P., Guerrini, L., Zuecco, G., Pezzuolo, A. (eds) Biosystems Engineering Promoting Resilience to Climate Change - AIIA 2024 - Mid-Term Conference. MID-TERM AIIA 2024. *Lecture Notes in Civil Engineering, Vol 586,* pp. 807-815. Springer, Cham. https://doi.org/10.1007/978-3-031-84212-2_100

[11] Mircea, C., Nenciu, F., Vlăduț, V., Voicu, G., Gageanu, I., Cujbescu, D. (2020). Increasing the performance of cylindrical separators for cereal cleaning, by using an inner helical coil, *INMATEH - Agricultural Engineering, Vol. 62*(3), pp. 249-258, https://doi.org/10.35633/inmateh-62-26.

[12] Mirzazadeh, A., Abdollahpour, S. Hakimzadeh, M. (2022). Optimized Mathematical Model of a Grain Cleaning System Functioning in a Combine Harvester using Response Surface Methodology. *Acta Technol. Agric*, *Vol. 25*, pp. 20-26. https://doi.org/10.2478/ata-2022-0004

[13] Schramm, M., Tekeste, M. Z. (2022). Wheat straw direct shear simulation using discrete element method of fibrous bonded model. *Biosystems engineering, Vol. 213*, pp. 1-12. https://doi.org/10.1016/j.biosystemseng.2021.10.010

[14] Shi, R., Dai, F., Zhao, W., Liu, X., Wang, T., Zhao, Y. (2022). Simulation Optimization and Experiment on Compound Cleaning System of Hilly Area Flax Combine Harvester (丘陵山地胡麻联合收获机复式清选系统仿真优化与试验). *Transactions of the Chinese Society for Agricultural Machinery*, *Vol. 53*(8), pp. 93-102+113. *(In Chinese)*. http://dx.doi.org/710.6041/j.issn.1000-1298.2022.08.010

[15] Shu, C., Yang, J., Liao, Q., Wan, X., Yuan, J. (2024). Design and experiment of guide-type dual-cyclone separation cleaning device for rapeseed combine harvester (油菜联合收获导流式双筒旋风分离清选装置设计及试验). *Journal of Jilin University (Engineering and Technology Edition)*, *Vol. 54*(6),

pp. 1807-1820. *(In Chinese)*. https://doi.org/10.13229/j.cnki.jdxbgxb.20220860

[16] Wan, X., Liao, Q., Xu, Y., Yuan, J., Li, H. (2018). Design and evaluation of cyclone separation cleaning devices using a conical sieve for rape combine harvesters. *Applied Engineering in Agriculture*, *Vol. 34*(4), pp. 677-686. https://doi.org/10.13031/aea.12502

[17] Wiącek, J., Parafiniuk, P., Molenda, M., Horabik, J., Gallego, E. (2023). DEM study of microstructural effects in friction of wheat on corrugated steel surface. *Tribology International, Vol. 183*: 108435. https://doi.org/10.1016/j.triboint.2023.108435

[18] Zhao, H., Li, X., Zhao, Y., Li, S., Diao, P. (2024). Simulation analysis and experiment of cleaning mechanism for track-type combine harvester based on CFD-DEM. *INMATEH - Agricultural Engineering, Vol. 74*(3), pp. 603-614, https://doi.org/10.35633/inmateh-74-54

[19] Zhou, B., Ma, S., Li, W., Wu, Z., Qian, J., Huo, P., Yang, S. (2025). CFD-DEM coupling simulation and parameter optimisation of sugarcane harvester extractor. *Biosystems Engineering, Vol. 250*, pp. 80-93. https://doi.org/10.1016/j.biosystemseng.2024.12.003